Available online at www.sciencedirect.com

ScienceDirect

journal homepage: www.JournalofSurgicalResearch.com

Real time shear waves elastography monitoring of thermal ablation: *in vivo* evaluation in pig livers

A. Mariani, MD,[a,d,*] W. Kwiecinski, PhD,[b] M. Pernot, PhD,[b] D. Balvay, PhD,[a] M. Tanter, PhD,[b] O. Clement, MD, PhD,[a,c] C.A. Cuenod, MD, PhD,[a,c] and F. Zinzindohoue, MD, PhD[a,d]

[a] *Laboratoire de recherche en imagerie, INSERM, UMR 970, Paris Cardiovascular Research Center, Université Paris Descartes, Sorbonne Paris Cité, Paris, France*

[b] *Laboratoire de recherche en imagerie, Institut Langevin, Ecole Superieure de Physique et de Chimie, Industrielles de Paris (ESPCI) ParisTech, CNRS UMR 7587, INSERM U979, Paris, France*

[c] *Department of Radiology, Assistance Publique-Hôpitaux de Paris, Hôpital Européen Georges Pompidou, Paris, France*

[d] *Department of Digestive and General Surgery, Assistance Publique-Hôpitaux de Paris, Hôpital Européen Georges Pompidou, Paris, France*

ARTICLE INFO

Article history:
Received 11 April 2013
Received in revised form
30 October 2013
Accepted 30 December 2013
Available online 4 January 2014

Keywords:
Elastography
Shear waves
Liver
Pigs
Thermal ablation
Coagulation necrosis
Radiofrequency

ABSTRACT

Background: Thermal ablation is a widely used minimally invasive treatment modality for different cancers. However, lack of a real-time imaging system for accurate evaluation of the procedure is one of the reasons of local recurrences. Shear waves elastography (SWE) is a new ultrasound (US) imaging modality to quantify tissue stiffness. The aim of the study was to assess the feasibility and accuracy of US elastography for quantitative monitoring of thermal ablation and to determine the elasticity threshold predictive of coagulation necrosis.

Methods: A total of 29 *in vivo* thermal lesions were performed in pig livers with radiofrequency system. SWE and B-mode images were acquired simultaneously. Liver elasticity was quantified by using SWE data and expressed in kilopascal. After the procedure, pathologic analysis of treated tissues was compared with US images. The sensitivity and positive predictive value of the SWE maps of tissue elasticity were calculated and compared with the boundaries of the pale coagulation necrosis areas found at pathology.

Results: The liver mean elasticity values before and after thermal therapy were 6.4 ± 0.3 and 38.1 ± 2.5 kPa, respectively ($P < 0.0001$). For a threshold of 20 kPa, sensitivity (i.e., the rate of pixels correctly detected as necrosed tissue) was 0.8, and the positive predictive value (i.e., the rate of pixels in the elastographic map >20 kPa that actually developed coagulation necrosis) was 0.83.

Conclusions: Tissue areas with coagulation necrosis are significantly stiffer than the surrounding tissue. SWE permits the real-time detection of coagulation necrosis produced by radiofrequency and could potentially be used to monitor US-guided thermal ablation.

* *Corresponding author*. Department of Digestive and General Surgery, Assistance Publique-Hôpitaux de Paris, Hopital européen Geoprges Pompidou, 20 rue Leblanc, 75015 Paris. Tel.: +33 1 56 09 35 34; fax +33 1 53 98 79 52.
E-mail address: a.mariani@hotmail.fr (A. Mariani).

0022-4804/$ – see front matter © 2014 Elsevier Inc. All rights reserved.
http://dx.doi.org/10.1016/j.jss.2013.12.024

1. Introduction

Thermoablative procedures have become a standard alternative to surgical resection for many liver tumors [1–3]. These minimally invasive therapies involve applying thermal energy to a probe inserted into the tumor mass to produce coagulation necrosis [4]. The safety and effectiveness of these therapies have been widely investigated [5], nevertheless high local recurrence rates have been reported [6]. Because of its low cost and wide availability even for surgeons during laparotomy or laparoscopy, ultrasonography is the preferred modality for image guidance [7]. Indeed, the heating process during thermal ablation leads to the production of steam bubbles that are seen as a transient hyperechoic zone, and these artifacts are commonly used as a surrogate marker of target destruction [8]. However, ultrasound (US) imaging is very imprecise and could be responsible for incomplete tumor ablation. Therefore, a robust and specific real-time imaging method to detect coagulation and precisely monitor the thermal ablation procedure is required. The thermal dose deposition could be monitored with real-time magnetic resonance (MR) imaging using temperature-sensitive sequences as this technique can accurately delineate the treated area and lower the risk of local recurrence [9,10]. However, MR imaging can be performed only within the MR magnet, which is associated with many technical obstacles and is expensive.

Alternatively, by quantifying the changes in elastic properties of the coagulated and untreated tissues, US elastography could allow the real-time and objective visualization of the thermal lesion boundaries and improve the accuracy of thermal ablation [11].

Indeed, during thermal ablation, coagulation, which involves protein denaturation and tissue dehydration, increases tissue stiffness [12]. Protein denaturation occurs almost instantaneously at temperatures above 60°C, whereas water vaporization, the main source of artifacts in B-mode ultrasonography, occurs above 100°C. According with the "thermal dose concept" [13], a thermoablative procedure with enough energy deposit to cause tissue coagulation necrosis without water vaporization could allow monitoring tissue elasticity without US artifacts. Tissue elasticity changes after coagulation have been measured using various US elastography techniques including static elastography [14,15], sonoelastography, and acoustic radiation force based techniques [16,17]. However, among those techniques, US shear waves elastography (SWE) is the only one that can provide quantitative maps of tissue stiffness [18,19] in real time. Quantitative estimation of tissue stiffness has been shown of major importance because tissue stiffness during tissue coagulation is directly linked to the thermal dose [10]. Therefore, SWE has the potential to visualize the location and the extent of a thermal lesion in real time [20].

To assess the feasibility and accuracy of quantitative elasticity monitoring during thermal therapy and to determine the elasticity threshold that predicts the formation of coagulation necrosis, we carried out an *in vivo* preclinical study in which SWE was used to map the coagulation necrosis areas produced in pig livers with a bipolar radiofrequency system.

2. Materials and methods

All procedures were approved by the University Committee for animal research of our institution and are in accordance with the guidelines issued by the National Institutes of Health for care of laboratory animals.

2.1. Animals and surgery

Twenty-nine thermal lesions (four to seven lesions per animal) were carried out in the liver of five Landrace pigs (weight range: 30–35 kg) using an open surgery approach in a surgical suite dedicated to large animals. Anesthesia was induced by ear vein intubation with a mixture of morphine hydrochloride (0.5 mg/kg; Morphine Lavoisier, France) and propofol (4 mg/kg; Fresenius, France) and maintained with isoflurane (1.5%–2.5% for 1 L/min oxygen inhalation; Forene, Abbott, France). The anesthetized animal was in dorsal recumbency on a warming blanket to preserve the body temperature, and then the abdomen was shaved for laparotomy. Vital parameters were monitored throughout the surgery.

2.2. Thermal lesions

After ventral midline laparotomy, two electrodes were inserted in the liver under US guidance, and coagulation necrosis was produced with a bipolar radiofrequency system connected to an electrosurgical generator (Force FX-8C electrosurgical generator; Valleylab, Tyco Healthcare, Switzerland). The generator power was 4 W, the radiofrequency was 470 kHz, and the distance between the two electrodes was always set to 7 mm. To ensure a good imaging reproducibility, we created a self-maintained therapy-imaging device that kept the imaging probe fixed while a translational mechanism allowed the insertion of the electrodes at the focal plane of the probe. A thermal "coagulation necrosis" lesion was created 1.5–2.5 cm beneath the liver surface in approximately 5 min without water vaporization or bubble formation.

2.3. Image collection

SWE and B-mode images were acquired with the US device Aixplorer (SuperSonic Imagine, Aix en Provence, France) using an 8 MHz linear probe. Images were taken before the procedure for reference, every 30 s during thermal ablation and every minute for 5 min at the end of the procedure. All images were taken in the focal plan. This plan was used as the reference for sample dissection.

First, B-mode images were used for electrode guidance. Then, SWE images were recorded using the SonicSoftware tool (Supersonic Imagine, Aix en provence, France). A color map in kilopascals, called elastogram, was obtained by calculating the Young's modulus. On the elastograms, using an adjustable color scale set between 0 kPa and 180 kPa, the stiff thermal lesion was depicted in red, whereas the surrounding tissue appeared in blue. Elastographic images and the corresponding B-mode images were acquired simultaneously and saved as static maps. To minimize motion

artifacts, images were acquired at the end of the expiratory phase of the respiratory cycle.

2.4. Exclusion criteria

An initial liver elasticity value >10 kPa was an exclusion criterion because such high value before any treatment revealed an artifact due to liver compression by the probe. When compression for technical reasons occurred, SWE measures cannot be considered reliable, and we chose to readjust probe and retake a reading. If not recognized during thermal procedure, we excluded lesion from the analysis.

2.5. Pathology

After *in vivo* US imaging, animals were euthanized by intravenous injection of 100 mg/kg sodium pentobarbital. The livers were resected and sliced in the focal plan. Gross examination of each lesion was performed in the same position and orientation in which it was previously imaged. Specimens were photographed beside a millimeter ruler. In accordance with previous reports [21,22], typical macroscopic thermal lesions with a central "white zone" (Wz) of coagulation necrosis surrounded by a peripheral, hyperemic "red zone" (Rz) within the native liver tissue were found (Fig. 1). A pathologist examined each region of interest to macroscopically differentiate the Wz and Rz areas. Specimens were then preserved in 10% formalin solution for microscopic analysis. Representative tissue samples were embedded in paraffin and stained with hematoxylin–eosin–safran.

2.6. Image analysis

SWE and pathology images were analyzed using a homemade software program written in Matlab (Mathworks, Natick, MA). For pathology photographs, the K-means clustering was used to automatically segment the Wz only. The Rz contained a large amount of red blood cells and did not always correspond to complete coagulation necrosis.

Raw data were used to analyze the elastographic maps. A region of interest was manually positioned at the lesion location; then, tissue stiffness was calculated before and after thermal ablation, and the mean elasticity values compared. Moreover, a new contour map (Fig. 2) was built by dividing the pixels in zones corresponding to 5 kPa of elasticity, from 15 to 60 kPa. The contours of thus created elasticity zones were considered as potential thresholds and tested in correlation with the *in vivo* findings. Indeed, after semiautomatic rigid registration of the elastographic and pathology image segmentation, the validity of the elastographic prediction was assessed by using a pixel-by-pixel analysis and by classifying the pixels in true positive, false positive and false negative, according to Figure 3. Areas that were classified as stiff (i.e., above each threshold in kilopascal) and that overlapped with the coagulation necrosis were considered as true positive. Segmented coagulation areas that were not covered by the elastographic map were considered as false negative. Areas above each threshold in kilopascal without necrosis were considered as false positive. The positive predictive value (PPV) and sensitivity (Se) were calculated for each threshold.

A radiologist (C.A.C.) with 20 y of experience interpreted blindly the B-mode images that corresponded to the studied SWE images and tried to outline the lesion boundaries, without knowledge of the elastographic maps. He knew a thermal ablative procedure had been performed following a protocol that avoided water vaporization and steam bubble formation. His mapping was estimated by using the NIH ImageJ software (National institutes of health) and compared with the surgical specimens.

2.7. Statistical analysis

Statistical analyses were performed using Matlab. The mean elasticity values of the thermal lesion areas and their respective standard deviations were calculated. Elasticity values before and after ablation were compared with the two-sided Student *t*-test. The Bland-Altman graphical method was used to detect the presence of systematic bias and measurements outside of the 95% confidence interval. $P < 0.05$ was considered statistically significant.

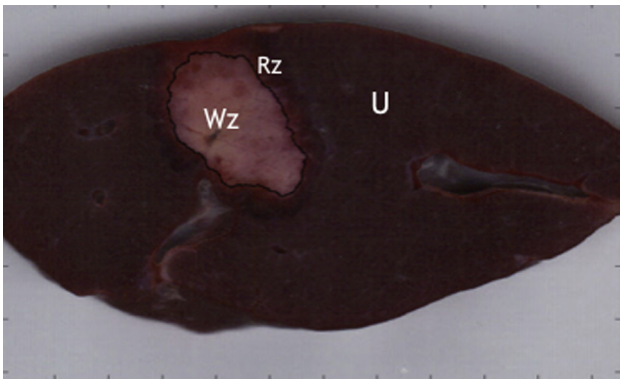

Fig. 1 – Pathologic standard features of a thermal lesion in macro specimen, with segmented Wz of necrosis coagulation, Rz with red blood cells, and untreated healthy tissue. (Color version of figure is available online.)

3. Results

Three lesions were excluded because of a pretreatment liver elasticity value >10 kPa. The 26 remaining areas of thermal lesions had a mean elasticity value of 6.4 ± 0.3 kPa before heating and of 38.1 ± 2.5 kPa ($P < 0.0001$) after the procedure that induced coagulation necrosis (Fig. 4).

3.1. Pathologic analysis

All thermal lesions showed the expected pathologic features, and the Wz and Rz could be clearly differentiated in all cases. The Rz thickness was 0.8–1.5 mm and the mean Wz area measured was 75.1 ± 20 mm^2 (40.5–131.3 mm^2).

3.2. Microscopic analysis

At low magnification (×5), the cell architecture of the Wz, Rz, and normal untreated tissue was clearly different. At higher

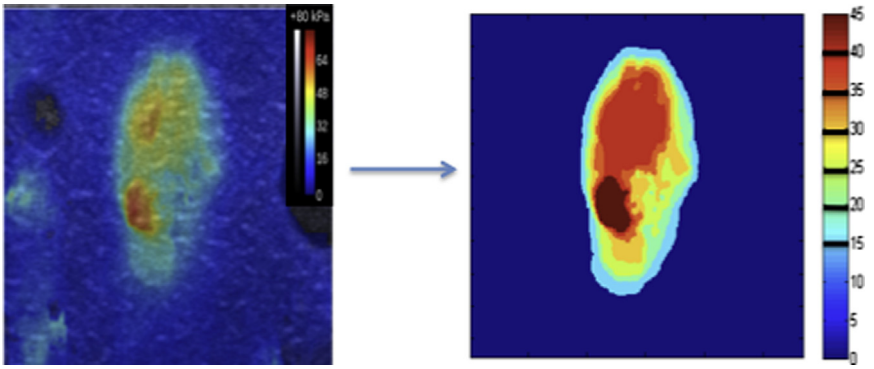

Fig. 2 – Elastographic map of a thermal lesion obtained by Aixplorer and pixel-by-pixel rebuilt contour map in Matlab (color scale in kilopascal). Core of this lesion did not exceed 45 kPa. (Color version of figure is available online.)

magnification (×40), conventional hematoxylin–eosin–safran staining did not show prominent changes in the Wz other than a lighter staining of the tissue with faintly stained nuclei and distortion of the sinusoidal architecture [23]. The Rz appeared as congestive tissue with a large amount of red blood cells.

3.3. *B-mode image analysis*

The expert radiologist did not detect any lesion in three cases (11.5%), could determine only incompletely the lesion boundaries in 16 cases (61.5%) and completely outlined what he considered to be the lesions in seven cases (27%). The mean surface difference between the Wz in the gross specimens and the lesion area delimited by the radiologist in B-mode images was 42.5%.

3.4. *Prediction of accurate visualization of coagulation necrosis*

Se and PPV were calculated for different elasticity thresholds as described in section Material and Methods. Figure 5 shows the Se–PPV couples for the different studied elasticity thresholds. Above 30 kPa, PPV was higher than 0.93 but was associated with Se values as low as 0.5. The curves showed that a 20 kPa threshold gave the best compromise between Se and PPV (0.8 and 0.83, respectively). The Bland-Altman method showed no bias as only one measurement was outside the 95% confidence interval. The estimated ablation area size on elastographic maps was very close to the Wz size (0.022 ± 0.22 cm^2 for bias $\pm$ standard deviation) with a confidence interval between −0.413 and 0.459 compared with the mean size of the lesions (0.751 cm^2).

4. Discussion

Real-time monitoring of thermal ablation by quantitative US elastography is technically feasible. In the core of the thermal lesion, stiffness quantified by US elastography is 6–8 times higher than in the surrounding healthy tissue, because of protein coagulation. An accurately determined elasticity threshold might help visualizing the boundaries of the created thermal lesion. Indeed, using an elasticity threshold of 20 kPa

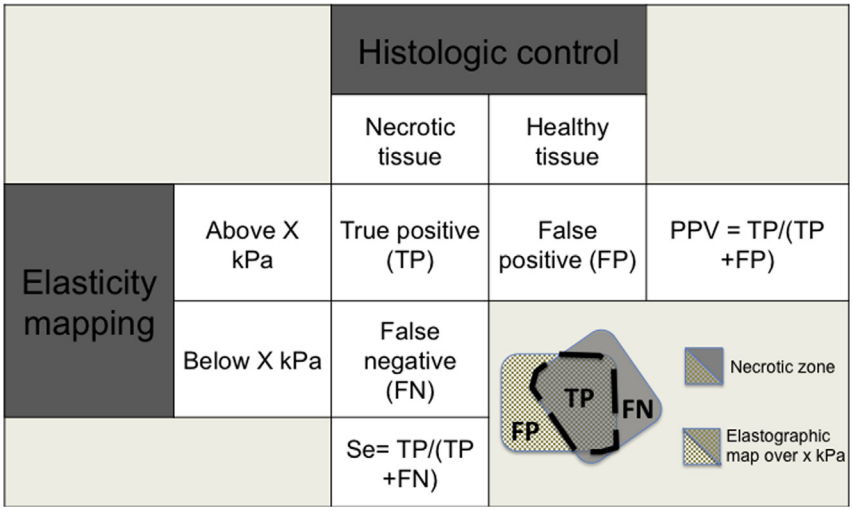

Fig. 3 – Scheme of data analysis. (Color version of figure is available online.)

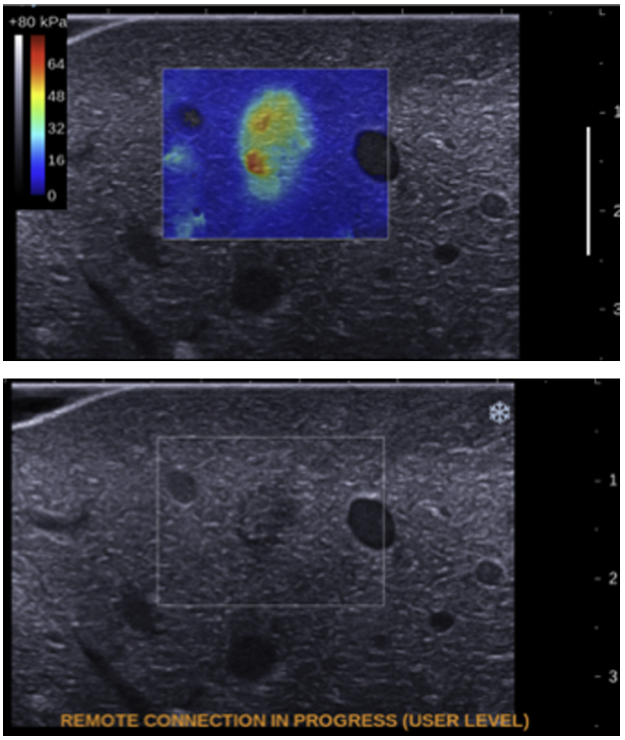

Fig. 4 – SWE map (top) and B-mode corresponding image (bottom) after thermal lesion creation T = 5 min. A stiff lesion could be seen in SWE, whereas a fuzzy hypo echogenic area could be seen in B-mode image. Gross pathology found a typical pattern of Wz and Rz. (Color version of figure is available online.)

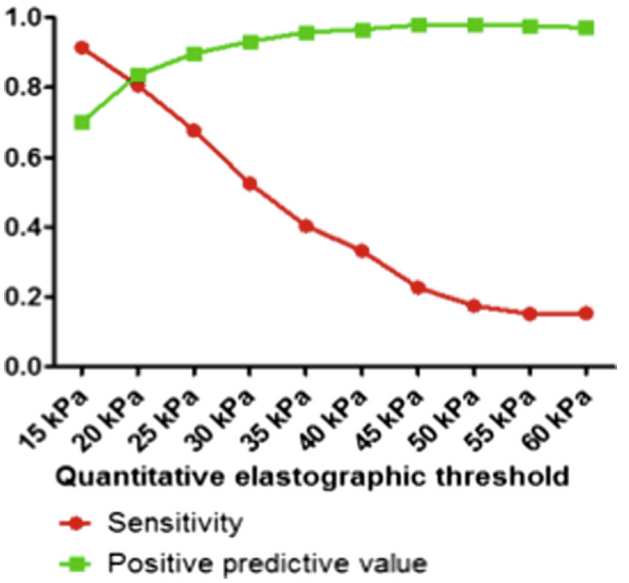

Fig. 5 – Se and PPV analysis of different quantitative elasticity threshold. (Color version of figure is available online.)

(two times higher than the native liver elasticity), we could predict cell necrosis with a PPV of 0.83 and Se of 0.8. Satisfactory clinical results using MR temperature mapping have also been reported [9,24], but they are associated with the classical MR drawbacks in terms of costs and availability. Due to the lack of accessibility to such MR systems in our country, we wished to test an US technique, less expensive and directly available in the operative room for surgeons or radiologists. Moreover, with MR temperature imaging, coagulation maps were estimated indirectly by computing the thermal dose. In contrast, tissue stiffness is an intrinsic property, which reflects the tissue organization at cellular and macroscopic level, and thus pathophysiological changes that occur during coagulation.

A radiologist with experience in liver US imaging and liver radiofrequency procedures under B-mode guidance in humans could not clearly delineate thermal ablative lesions in 70% of the cases even in the absence of artifacts (gas bubble formation) that can alter US imaging and real-time estimation of the size of the thermal lesion [25]. Although B-mode ultrasonography is the most commonly used guidance method for liver thermal ablative procedures, it is not precise enough for real-time monitoring of thermal ablation and prediction of the extent of coagulation necrosis [26].

Automatic segmentation of the liver specimens was used to avoid interindividual differences. The pathologic findings showed a classical Wz of coagulation necrosis surrounded by a peripheral congestive Rz with a large amount of red blood cells. Like in previous reports [21,22,27], we defined as "coagulation necrosis" only areas with macroscopic features that were highly predictive of irreversible thermal cell damage. Histologic evidence of necrosis is commonly found *in vivo* 24–36 h after hepatocyte ischemic injury, and mitochondrial abnormalities are the earliest finding [28]. At the early stage analyzed in this study, only immunohistochemical vital dyes could clearly demonstrate loss of vitality immediately after thermal ablation [29–31].

This study has several limitations. First, because of the small sample size and the creation of standardized lesion, the findings should be cautiously interpreted. Second, healthy livers were treated because no pig liver cancer cell lines are currently available. Thus, the effectiveness and accuracy of elastography mapping remains to be evaluated using pseudotumor models [11] or cirrhotic liver. SWE might confirm MR-elastography findings that malignant tumors were stiffer than human healthy liver with an elasticity around 10 kPa [32] and 2 kPa [33], respectively. Thanks to this contrast, it could be possible to apprehend coagulation necrosis at the margin of the tumor [11]. Finally, this study was designed to monitor thermal procedures during open abdominal surgery; however, as SWE can assess and measure deep tissue stiffness, it might be used also for percutaneous radiofrequency ablation. Further studies need to be performed to test this specific assumption.

5. Conclusions

The development of new imaging strategies to provide real-time assessment of the effectiveness of thermal procedures is an important issue for mini-invasive treatments, such as open or percutaneous ablative therapies. Completeness of a thermal ablation procedure is particularly difficult to determine in real time with the risk of leaving behind viable tumor cells. SWE is a new imaging modality that quantifies tissue

stiffness and that is mostly used for diagnosis [19,34]. Here, we show that areas of coagulation necrosis are significantly stiffer than the surrounding tissue and that their boundaries can be predicted with effectiveness and reproducibility using SWE, preclinically. In previous studies [11,35], US elastography has proven its interest and superiority compared with standard B-mode ultrasonography. Additional preclinical studies with pseudotumor models [36] are needed to validate this technique.

Acknowledgment

The authors wish to thank Julie Piquet, Martine Rancic, and Adrien Lalot from the Laboratoire de recherches biochirurgicales headed by Pr Menasché for their help with animal studies. This work was supported by funding from the Institut National du Cancer AND (INCa) and société française de radiologie (SFR). We also wish to thank Dr Meatchi from the HEGP Anapath Laboratory for carrying out the histologic analysis.

The authors have no conflict of interest.

REFERENCES

[1] Lencioni R, Crocetti L. Local-regional treatment of hepatocellular carcinoma. Radiology 2012;262:43.
[2] Solbiati L, Ahmed M, Cova L, Ierace T, Brioschi M, Goldberg SN. Small liver colorectal metastases treated with percutaneous radiofrequency ablation: local response rate and long-term survival with up to 10-year follow-up. Radiology 2012;265:958.
[3] Van Tilborg AAJM, Meijerink MR, Sietses C, et al. Long-term results of radiofrequency ablation for unresectable colorectal liver metastases: a potentially curative intervention. Br J Radiol 2011;84:556.
[4] Decadt B, Siriwardena AK. Radiofrequency ablation of liver tumours: systematic review. The Lancet Oncol 2004;5:550.
[5] Livraghi T, Solbiati L, Meloni MF, Gazelle GS, Halpern EF, Goldberg SN. Treatment of focal liver tumors with percutaneous radio-frequency ablation: complications encountered in a multicenter study. Radiology 2003;226:441.
[6] Reuter NP, Woodall CE, Scoggins CR, McMasters KM, Martin RCG. Radiofrequency ablation vs. resection for hepatic colorectal metastasis: therapeutically equivalent? J Gastrointest Surg 2009;13:486.
[7] Curley SA, Izzo F, Ellis LM, Nicolas Vauthey J, Vallone P. Radiofrequency ablation of hepatocellular cancer in 110 patients with cirrhosis. Ann Surg 2000;232:381.
[8] Goldberg SN, Grassi CJ, Cardella JF, et al. Image-guided tumor ablation: standardization of terminology and reporting criteria. Radiology 2005;235:728.
[9] Rempp H, Clasen S, Boss A, et al. Prediction of cell necrosis with sequential temperature mapping after radiofrequency ablation. J Magn Reson Imaging 2009;30:631.
[10] Rempp H, Hoffmann R, Roland J, et al. Threshold-based prediction of the coagulation zone in sequential temperature mapping in MR-guided radiofrequency ablation of liver tumours. Eur Radiol 2012;22:1091.
[11] Van Vledder MG, Boctor EM, Assumpcao LR, et al. Intraoperative ultrasound elasticity imaging for monitoring of hepatic tumour thermal ablation. HPB (Oxford) 2010;12:717.
[12] Brosses ES, Pernot M, Tanter M. The link between tissue elasticity and thermal dose in vivo. Phys Med Biol 2011;56:7755.
[13] Sapareto SA, Dewey WC. Thermal dose determination in cancer therapy. Int J Radiat Oncol Biol Phys 1984;10:787.
[14] Kallel F, Stafford RJ, Price RE, Righetti R, Ophir J, Hazle JD. The feasibility of elastographic visualization of HIFU-induced thermal lesions in soft tissues. Image-guided high-intensity focused ultrasound. Ultrasound Med Biol 1999;25:641.
[15] Souchon R, Rouviére O, Gelet A, et al. Visualisation of HIFU lesions using elastography of the human prostate in vivo: preliminary results. Ultrasound Med Biol 2003;29:1007.
[16] Fahey BJ, et al. In vivo guidance and assessment of liver radio-frequency ablation with acoustic radiation force elastography. Ultrasound Med Biol 2008;34:1590.
[17] Bercoff J, Pernot M, Tanter M, Fink M. Monitoring thermally-induced lesions with supersonic shear imaging. Ultrason Imaging 2004;26:71.
[18] Bercoff J, Tanter M, Fink M. Supersonic shear imaging: a new technique for soft tissue elasticity mapping. IEEE Trans Ultrason Ferroelectr Freq Control 2004;51:396.
[19] Athanasiou A, Tardivon A, Tanter M, et al. Breast lesions: quantitative elastography with supersonic shear Imaging—preliminary results. Radiology 2010;256:297.
[20] Arnal B, Pernot M, Tanter M. Monitoring of thermal therapy based on shear modulus changes: II. Shear wave imaging of thermal lesions. IEEE Trans Ultrason Ferroelectr Freq Control 2011;58:1603.
[21] Goldberg SN, Gazelle GS, Compton CC, Mueller PR, Tanabe KK. Treatment of intrahepatic malignancy with radiofrequency ablation: radiologic-pathologic correlation. Cancer 2000;88:2452.
[22] Pereira PL, Trübenbach J, Schenk M, et al. Radiofrequency ablation: in vivo comparison of four commercially available devices in pig livers. Radiology 2004;232:482.
[23] McGahan JP, Browning PD, Brock JM, Tesluk H. Hepatic ablation using radiofrequency electrocautery. Invest Radiol 1990;25:267.
[24] Lepetit-Coiffé M, Laumonier H, Seror O, et al. Real-time monitoring of radiofrequency ablation of liver tumors using thermal-dose calculation by MR temperature imaging: initial results in nine patients, including follow-up. Eur Radiol 2010;20:193.
[25] Chagnon S, Qanadli S, Lacombe P. [Percutaneous radiofrequency ablation of liver tumors]. Gastroenterol Clin Biol 2001;25:B85.
[26] Cha CH, Lee FT, Gurney JM, et al. CT versus Sonography for monitoring radiofrequency ablation in a porcine liver. AJR 2000;175:705.
[27] Kim Y, Rhim H, Lim HK, Lee MW, Park MJ. Coagulation necrosis induced by radiofrequency ablation in the liver: histopathologic and radiologic review of usual to extremely rare changes. Radiographics 2011;31:377.
[28] Rosser BG, Gores GJ. Liver cell necrosis: cellular mechanisms and clinical implications. Gastroenterology 1995;108:252.
[29] Gettman MT, Lotan Y, Corwin TS, et al. Radiofrequency coagulation of renal parenchyma: comparison of effects of energy generators on treatment efficacy. J Endourology 2002;16:83.
[30] Kim YN, Rhim H, Choi D, et al. The effect of radiofrequency ablation on different organs: ex vivo and in vivo comparative studies. Eur J Radiol 2011;80:526.
[31] Wennerberg AE, Nalesnik MA, Coleman WB. Hepatocyte paraffin 1: a monoclonal antibody that reacts with hepatocytes and can be used for differential diagnosis of hepatic tumors. Am J Pathol 1993;143:1050.
[32] Venkatesh SK, Yin M, Glockner JF, et al. MR elastography of liver tumors: preliminary results. AJR Am J Roentgenol 2008;190:1534.

[33] Lee DH, Lee JM, Han JK, Choi BI. MR elastography of healthy liver parenchyma: normal value and reliability of the liver stiffness value measurement. J Magn Reson Imaging; 2012. http://dx.doi.org/10.1002/jmri.23958.
[34] Evans A, Whelehan P, Thomson K, et al. Quantitative shear wave ultrasound elastography: initial experience in solid breast masses. Breast Cancer Res 2010;12:R104.
[35] Zhang M, Castaneda B, Christensen J, et al. Real-time sonoelastography of hepatic thermal lesions in a swine model. Med Phys 2008;35:4132.
[36] Eun D, Bhandari A, Boris R, et al. A novel technique for creating solid renal pseudotumors and renal vein-inferior vena caval pseudothrombus in a porcine and cadaveric model. J Urol 2008;180:1510.